International Journal of Remote Sensing
Vol. 26, No. 4, 20 February 2005, 661–681

Taylor & Francis
Taylor & Francis Group

A global analysis of urban reflectance

C. SMALL
Lamont Doherty Earth Observatory, Columbia University, Palisades, NY 10964, USA;
Email: small@LDEO.columbia.edu

(*Received 20 August 2002; in final form 10 November 2003*)

A comparative Spectral Mixture Analysis (SMA) of Landsat 7 Enhanced Thematic Mapper (ETM+) imagery for a collection of 28 urban areas worldwide provides a physical basis for a spectral characterization of urban reflectance properties. These urban areas have similar mixing space topologies and can be represented by three-component linear mixture models in both scene-specific and global composite mixing spaces. The results of the analysis indicate that the reflectance of these cities can be accurately described as linear combinations of High Albedo, Dark and Vegetation spectral endmembers within a two-dimensional mixing space containing over 90% of the variance in the observed reflectance. Only two of the 28 cities had greater than 10% median RMS misfit to the three-endmember linear model. The relative proportions of these endmembers vary considerably among different cities and within individual cities but in all cases the reflectance of the urban core lies near the dark end of a mixing line between the High Albedo and Dark endmembers. The most consistent spectral characteristic of the urban mosaic is spectral heterogeneity at scales of 10–20 m. In spite of their heterogeneity, built-up areas do occupy distinct regions of the spectral mixing space. This localization in mixing space allows spectrally mixed pixels in built-up areas to be discriminated from undeveloped land cover types. This provides a basis for mapping the spatial extent of human settlements using broadband optical satellite imagery collected over the past 30 years.

1. Introduction

Since the launch of Landsat 1 in 1972, the world's urban population has almost doubled (United Nations 2002). Although urban areas occupy a relatively small fraction of Earth's surface area, their extent, distribution and evolution have enormous impact on environmental and socio-economic dynamics worldwide (e.g. Berry 1990, Chameides *et al.* 1994). A variety of urban growth models have been developed (e.g. Nordbeck 1971, Batty and Longley 1994, Zanette and Manrubia 1997, Makse *et al.* 1998) but the spatially explicit data necessary to test and refine these models are relatively sparse. When available, multitemporal maps of urban extent are generally based on municipal administrative boundaries that rarely reflect the variations in land use related to the causes and effects of urban growth. A systematic quantitative measure of the spatial extent and growth of urban areas would facilitate the development and testing of urban growth models by providing comparisons of urban morphology and growth dynamics in different physical, cultural and socio-economic settings.

Moderate resolution (10–100 m) optical sensors provide an underutilized 30-year record of global urban evolution at spatial scales sufficient to distinguish built-up

International Journal of Remote Sensing
ISSN 0143-1161 print/ISSN 1366-5901 online
http://www.tandf.co.uk/journals
DOI: 10.1080/01431160310001654950

urban areas from other land cover types. This satellite imagery is routinely used to provide visual depictions of urban areas but comparative quantitative analyses of urban land cover are relatively rare. Mapping urban land cover is important because it reflects land-use patterns related to socio-economic activities that impact the surrounding environments (e.g. Forster 1983, Jensen and Cowen 1999). Despite its fundamental importance, urban land cover has not been characterized to the same extent that other land cover types have. In order to quantify the extent and evolution of urban areas with optical sensors it is necessary to understand the physical characteristics that distinguish urban areas from other types of human modified and undeveloped land surfaces. These physical characteristics determine the nature of the radiance field measured by sensors and therefore determine what can and cannot be measured remotely. Comparative analyses are especially important because of the diverse physical, cultural and socio-economic factors that determine the physical form of urban areas. A systematic physical characterization of optical reflectance properties of urban areas could therefore facilitate a self-consistent global mapping of urban extent. Cities are clearly delineated in moderate resolution imagery but their recognition depends, in part, on a complex combination of visual cues related to differences in colour and texture as well as the recognition of anthropogenic features like street grids. The question this study seeks to address is whether or not urban areas have distinctive spectral properties that distinguish them from other land cover types.

One of the primary obstacles to urban land cover classification is the diversity and spectral heterogeneity of urban reflectance. Compared to other land cover types, urban reflectance is extremely variable at a variety of spatial scales. Spectral heterogeneity at scales comparable to the Ground Instantaneous Field Of View (GIFOV) of an optical sensor results in a preponderance of spectrally mixed pixels. Mixed pixels are problematic for statistical classification methods because most algorithms are predicated on the assumption of spectral homogeneity within a particular class of land cover. The classification task is often further complicated by physical inconsistencies between the thematic classes sought and the reflectance properties that can be discriminated with moderate resolution broadband sensors. Urban areas provide examples of spectrally diverse, scale-dependent thematic classes containing large numbers of pixels that are spectrally indistinguishable from other land cover classes. The diversity of land cover types and scales in the urban mosaic therefore results in high rates of misclassification between urban and other land cover classes. Combining spectral, textural and ancillary information can improve classification accuracy (e.g. Stefanov *et al.* 2001) but a physical characterization of reflectance is still necessary to accommodate the physical processes that influence the upwelling radiance measured by optical sensors. Several recent studies have used physical rather than statistical classifications of urban land cover in individual cities with some degree of success (e.g. Kressler and Steinnocher 1996, 2000, Small 2001a, Rashed *et al.* 2002). This analysis attempts to generalize the approaches of these previous studies in a single analysis of a wide variety of urban areas.

The objective of this study is to develop a robust, quantitative physical characterization of the reflectance properties of urban mosaics. This task is complicated by two distinct types of variability in urban reflectance. Intraurban spectral variability is a result of the diversity of building materials and land covers present in the urban mosaic at different spatial scales. Interurban variability in

reflectance is a result of socio-economic, cultural, historical and environmental differences among cities. Factors such as building materials, physical environment, urban planning constraints and historical evolution influence differences in overall reflectance patterns observed between cities worldwide. This study uses the concepts of Spectral Mixture Analysis (SMA) to provide self-consistent physical descriptions of a variety of cities in order to determine what, if any, reflectance characteristics can be used to distinguish urban land cover in moderate resolution optical imagery.

2. Reflectance scale and spectral mixing

The characteristic spatial scale of surface reflectance patterns in the built environment is comparable to the GIFOV of most operational multispectral sensors in use today. Two-dimensional spatial autocorrelation of 1 m Ikonos imagery in 14 cities of varying size and setting indicates that the characteristic spatial scale on which visible/near-infrared reflectance decorrelates is 10–20 m (Small 2003). This explains the preponderance of mixed pixels observed in 30 m Landsat imagery of urban areas. This spectral mixing within the urban mosaic is also what often prevents hard classification algorithms from producing accurate results. The spectral heterogeneity at pixel scale violates the cardinal assumption of most statistical classification algorithms (e.g. maximum likelihood) wherein each thematic class is assumed to be both spatially and spectrally homogeneous relative to the spectral differences among classes. In order to characterize urban reflectance in a physically meaningful and sufficiently robust way, it is necessary to accommodate the fact that moderate resolution sensors will generally image a combination of discrete surface reflectances and represent the upwelling radiance field in the form of a mixed pixel.

Spectral Mixture Analysis (SMA) provides a systematic way to quantify spectrally heterogeneous urban reflectance. SMA is based on the observation that, in many situations, radiances from surfaces with different 'endmember' reflectances mix linearly in proportion to area within the instantaneous field of view (IFOV) (Nash and Conel 1974, Singer and McCord 1979, Singer 1981, Johnson *et al.* 1983). This observation has made possible the development of a systematic methodology for SMA (Adams *et al.* 1986, 1989, Smith *et al.* 1990, Gillespie *et al.* 1990) that has proven successful for a variety of quantitative applications with multispectral imagery (e.g. Pech *et al.* 1986, Smith *et al.* 1990, Adams *et al.* 1995, Roberts *et al.* 1998, Elmore *et al.* 2000). If a limited number of distinct spectral endmembers are known *a priori* it is possible to define a 'mixing space' within which mixed pixels can be described as linear mixtures of the endmembers. Given sufficient spectral resolution, a system of linear mixing equations can be defined and the best fitting combination of endmember fractions can be estimated for the observed reflectance spectra (Boardman 1989, Johnson *et al.* 1985, Smith *et al.* 1985). The strength of the SMA approach lies in the fact that it explicitly takes into account the physical processes responsible for the observed radiances and therefore accommodates the existence of mixed pixels. This discussion provides only a brief summary of urban SMA. A more detailed discussion of the theory, analysis and validation for urban areas is given by Small (2001a) and the works cited above.

This study is based on a diverse collection of cities spanning a range of environmental, cultural and socio-economic settings. The analyses are conducted on a set of 28 Enhanced Thematic Mapper (ETM+) images acquired by Landsat 7 between 1999 and 2001. This quasi-random selection was gleaned from the Landsat

7 archive at the University of Maryland's Global Land Cover Facility. The cities were chosen on the basis of area, diversity and image quality. All analyses were conducted on exoatmospheric reflectance estimates. No atmospheric corrections have been applied. For each city, a 30 km × 30 km image was chosen to represent the urban area and as wide a variety of surrounding land covers as possible (figure 1). In most cases, the 900 km^2 image contained all of the built-up area and varying amounts of surrounding land covers. In only two cases (New York and Sao Paulo) was the built-up area too large to be contained in the subscene. In these cases, the scene was chosen to cover the city centre as well as some land cover representative of the surrounding areas.

3. Urban mixing spaces

This analysis characterizes urban reflectance in the context of the regional mixing space that includes both the built-up urban area and the variety of regional land cover types within and surrounding the city. Continuous fractions can represent different mixtures of land cover corresponding to different types of urban land use as well as the urban-rural gradient in land cover. The true dimensionality of the mixing space is determined by the number of spectrally distinct endmembers present in the urban mosaic. The apparent dimensionality of the mixing space is determined by the number of spectral endmembers that can actually be distinguished by the sensor. The apparent dimensionality is therefore constrained by the number of spectral bands available as well as the wavelengths spanned by the bands. The limited spatial and spectral resolution of the ETM+ sensor results in a projection of a true high dimensional mixing space onto a lower dimensional representation constrained by the ability of the sensor to discriminate different surface reflectances at GIFOV scales. Analyses of AVIRIS hyperspectral imagery suggest that some urban areas have as many as 30–50 spectral dimensions (Green and Boardman 2000, Small 2001b) but the TM and ETM+ sensors can resolve only six of these dimensions at most. A central question of this analysis is whether these six dimensions provide an adequate basis for a systematic characterization of urban reflectance. Is the information content provided by the Landsat sensor sufficient to discriminate between urban areas and other land cover types in a consistent manner? The fact that an experienced interpreter can recognize urban areas in Landsat imagery suggests that this is the case but visual interpretation is based on a complex combination of spectral and textural cues that generally prove extremely difficult to simulate with machine-based algorithms.

The basis of the SMA is the variance partition and mixing space characterization provided by a principal component transformation of the multispectral imagery. The eigenvalue distribution provides a quantitative estimate of the variance partition between the signal and noise dominated principal components of the image (figure 2). The multidimensional feature space of the low order principal components represents the spectral mixing space that can be used to describe the spectral mixtures as combinations of spectral endmembers. In this analysis, a Minimum Noise Fraction (MNF) principal component transformation is used. The MNF transformation implemented in the ENVI image processing software is analogous to the Maximum Noise Transformation described by Green *et al.* (1988) but differs in ordering of the principal components from high to low signal variance (RSI 2000). With Landsat imagery, the MNF transformation usually produces principal components similar to those resulting from a traditional covariance-based PC rotation but offers the added benefit of normalizing the eigenvalues relative to

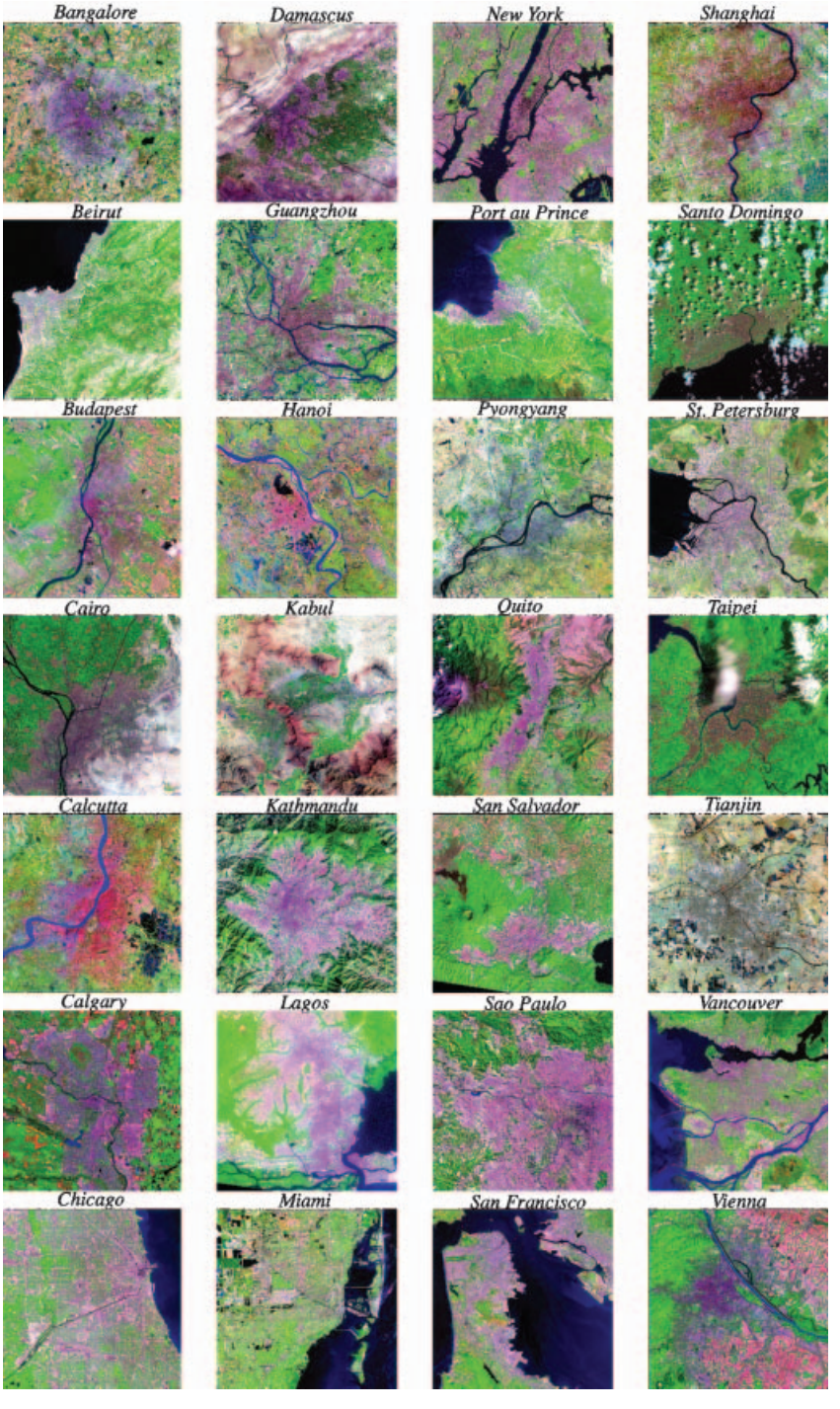

Figure 1. Visible/infrared false colour composites of urban Landsat 7 imagery. ETM+ bands 7, 4 and 2 (RGB) emphasize contrast between soil, vegetation, high albedo and dark land covers at 30 m spatial scales. A 2% linear stretch has been applied to each image so the variation in the colour of the built-up areas is influenced by the distribution of reflectances in the surrounding areas. A higher resolution colour version of this figure is available online at www.LDEO.columbia.edu/~small/Urban.html

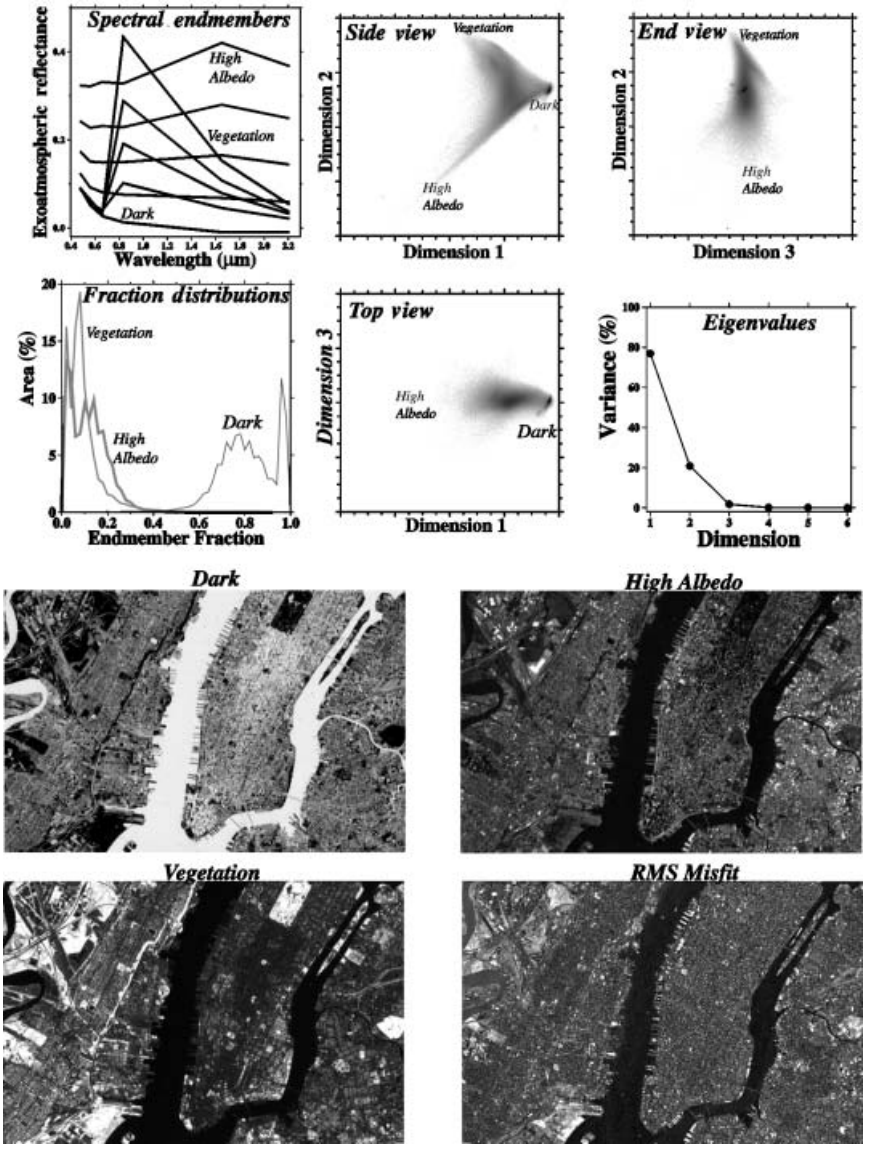

Figure 2. A SMA example for New York City. The density shaded scatter plots show orthogonal projections of the spectral mixing space formed by the three low order principal components. The eigenvalues show the variance associated with each dimension (principal component) of the mixing space. The two primary dimensions in the side view contain 97% of the total scene variance suggesting that the mixing space can be described with a three-endmember linear mixing model. The reflectance vectors show the spectra of the three endmembers (bold) as well as intermediate binary mixture spectra (grey) from points on the two sharply defined linear edges of the mixing space. Inversion of the three-endmember linear mixing model for each pixel results in the fraction and misfit images shown below. Each fraction ranges from 0 (black) to 1 (white) and the misfits range from 0 to 0.1. The fraction distributions have distinct narrow peaks for the dark water bodies and emphasize the dominance of the Dark endmember. Spatial variations in vegetation fraction correspond to differences in abundance of street trees while the parks and wetlands are clearly delineated by the high vegetation fractions. Areas of exposed soil have higher misfits because the model contains no soil endmember.

the variance of the sensor noise estimate. For this analysis, all MNF transformations were applied using noise covariance statistics derived from a June 2000 ETM+ image of a large, clear lake at 3400 m elevation in the Peruvian highlands. Normalized eigenvalue distributions quantify the partition of variance among the principal components indicating how many spectral dimensions are required to represent the information content in the image. The larger eigenvalues are associated with the low order principal components representing the dominant reflectance patterns while the smaller eigenvalues are associated with the higher order principal components associated with the pixel scale variance commonly assumed to be noise. This assumption is obviously incorrect in urban areas but it will not detract from the results as this study focuses on the overall reflectance properties of urban areas rather than higher order endmembers. Scatter plots showing the two primary dimensions of the 28 individual images are shown in figure 3.

SMA of a single city can use local endmembers calibrated to specific land cover types within the image but in order to compare endmember fraction distributions of different cities it is necessary to estimate fractions relative to a common set of endmembers. This can be done either by radiometrically rectifying all of the scene-specific sets of endmembers bounding each individual mixing space (Small 2002) or by using a single set of endmembers for all inversions. In this analysis a common set of global endmembers is used to estimate fraction images for each urban area. The global endmember set is selected from the global mixing space shown in figure 4. This mixing space represents a combination of 18 of the 28 images used in this study. The 18 images were chosen to span the range of land cover types encompassed by the 28 images while minimizing redundancy and accommodating hardware limitations. The topology of the triangular mixing space in figure 4 is consistent with the mixing spaces of the individual images. The edge between the Vegetation and Low Albedo endmembers is straight, indicating linear binary mixing. The edge between the High and Dark endmembers is slightly convex and diffuse, revealing the presence of a fourth endmember and some nonlinear mixing along the 'grey axis' spanning the Dark and High Albedo endmembers. The tapering of the mixing space approaching the Vegetation endmember suggests that the vegetation fraction is well constrained by the linear model.

Spectral mixing spaces provide a self-consistent basis for comparison of urban reflectance characteristics. The similarity of the triangular mixing spaces shown in figure 3 indicates that the images in this study have a consistent mixing space topology. Although the distributions of mixed pixels within the mixing spaces vary considerably, the overall form is similar. The apexes of the mixing space corresponding to the spectral endmembers are generally well defined and the edges between the apexes are generally straight or concave. This suggests that the mixing among the endmembers is primarily linear. The variance partition given by the eigenvalue distributions in figure 5 indicates that the two-dimensional mixing spaces shown in figure 3 contain almost all of the spatially coherent information in the images. For comparison, the eigenvalues corresponding to the 1 km city centres show a greater dominance of the primary dimension and relatively greater contribution of the third dimension relative to the second dimension in the 30 km images. This reflects the diminishing contribution of the Vegetation endmember in the city centres as the mixing space is dominated by the grey axis between the High and Dark endmembers and influenced by the nonlinear mixing into the third dimension.

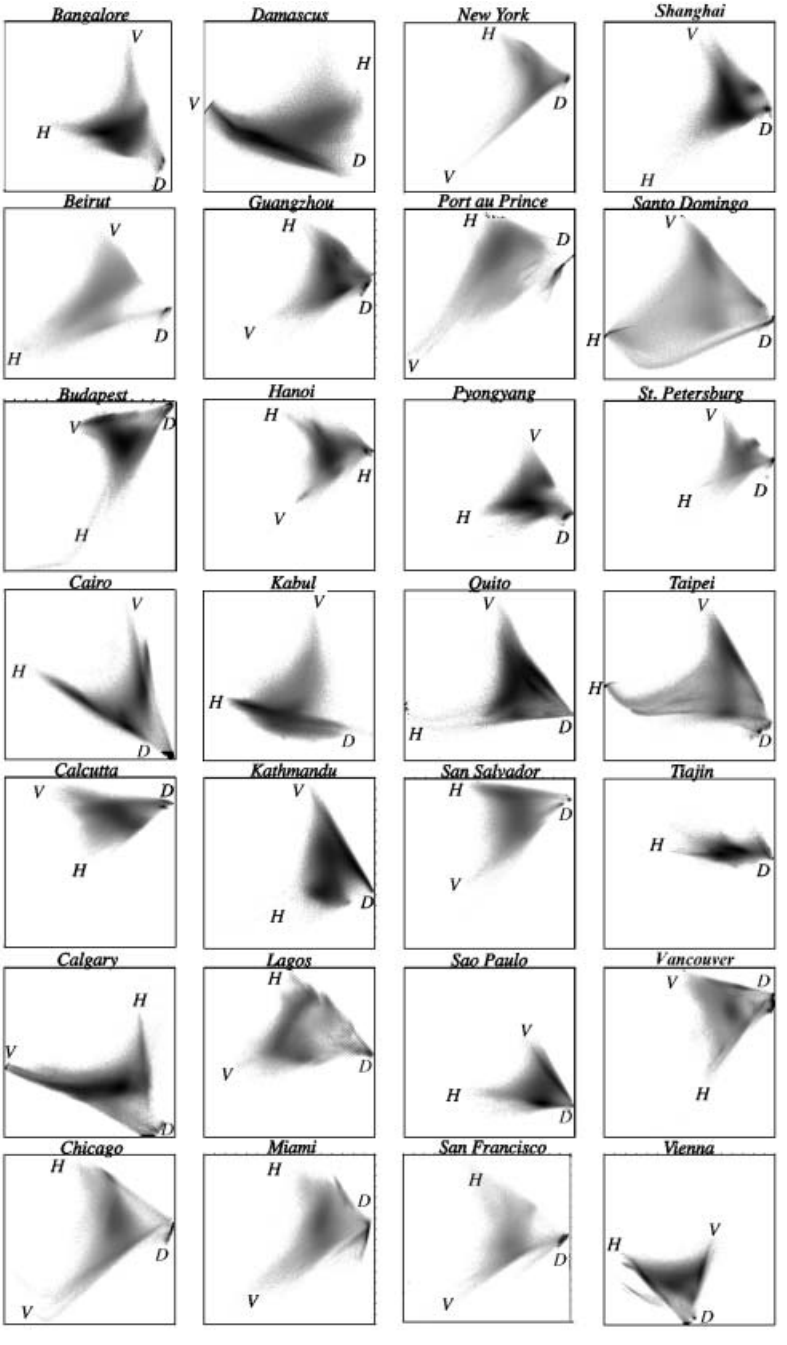

Figure 3. Spectral mixing spaces of the 28 urban areas and their surroundings shown in figure 1. Each two-dimensional mixing space is represented by a density shaded scatter plot of the two low order principal components of the corresponding image in figure 1. The pixels near the apexes of the scatter plot represent spectral endmembers while the darker interior regions represent a greater number of mixed pixels. The mixing spaces generally have a triangular form in the two primary dimensions. The pixels at the apexes consistently correspond to High Albedo, Dark and Vegetation endmembers. The small, dark clusters (generally at the right-most apex) correspond to water and deep shadow.

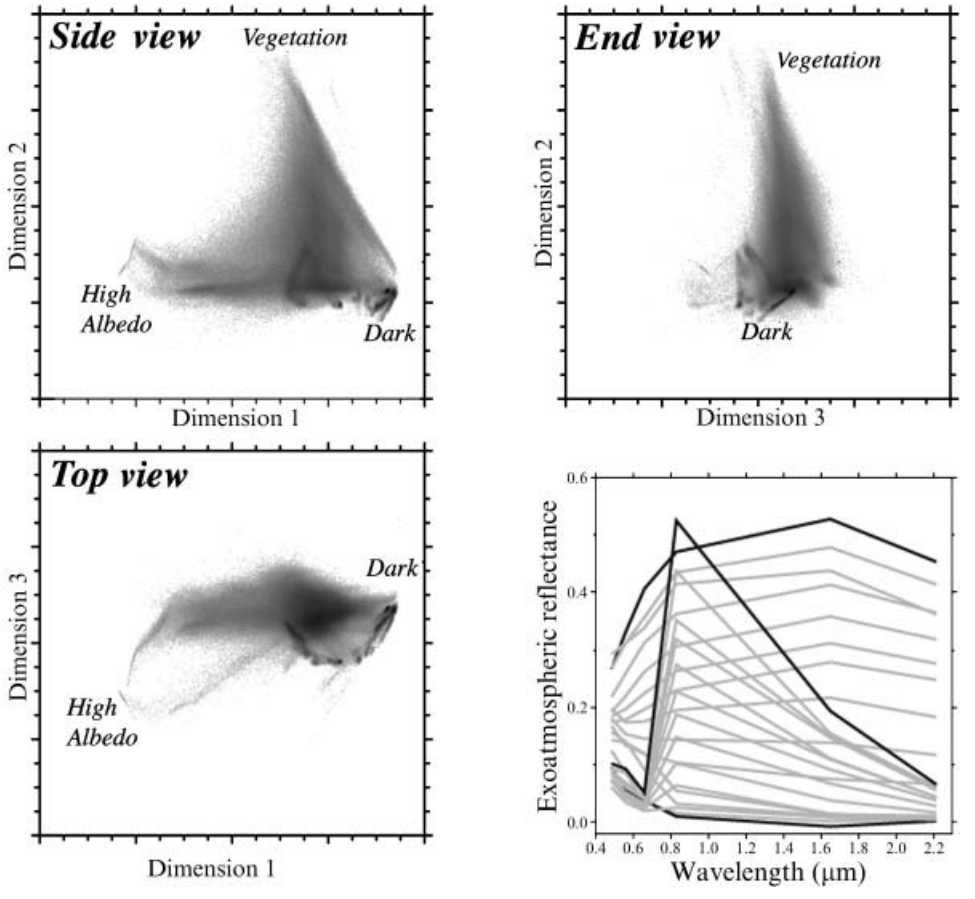

Figure 4. Global spectral mixing space and endmember reflectance vectors. Three orthogonal projections of the three low order dimensions show the familiar triangular mixing space with linear mixing between the Dark endmember and the Vegetation and High Albedo endmembers. The third dimension accounts for 3.5% of the variance corresponding primarily to the 'grey axis' between the High and Dark endmembers. The arcuate mode near the Dark endmember in the top view corresponds to different water body reflectances in the global composite. Endmember spectra are plotted in bold and binary mixtures from the two linear edges of the mixing space are shown in grey.

4. Spectral endmembers and linear mixture models

The comparative analysis shows that a wide variety of urban areas have similar spectral mixing spaces and might be described with a simple three-component linear mixture model. The consistency in the topology of the mixing spaces is reflected in the consistency of the spectral endmembers. Figure 6 shows exoatmospheric reflectance vectors for the three endmembers associated with the apexes of the primary two-dimensional mixing space. The Dark and Vegetation endmembers are remarkably consistent in light of the fact that no atmospheric corrections have been made. The High Albedo endmember is variable in amplitude but is generally convex upward with a peak at short wave infrared (SWIR) wavelengths.

The Dark endmember generally corresponds to deep shadow or clear water. In many cases, several different water bodies of differing reflectance can be resolved as distinct clusters near the low albedo (Dark) apex of the mixing space. In these cases,

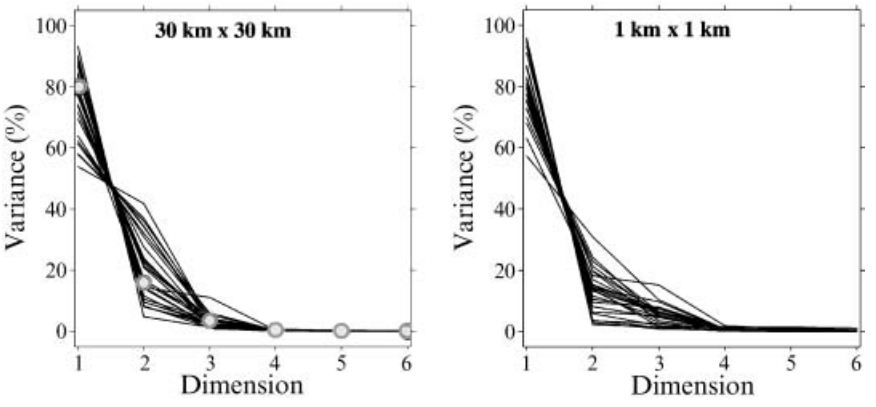

Figure 5. Variance partition and spatial scale. Normalized eigenvalue distributions show the partition of variance among the principal components for each 30 km × 30 km urban area and for 1 km × 1 km subscenes from the city centres. Eigenvalues corresponding to the principal components of the global dataset are shown by circles. The two low order principal components generally account for more than 90% of scene variance, indicating that the mixing spaces are primarily two-dimensional. The larger 30 km images generally have a greater percentage of variance in the first dimension as a result of the albedo contrast between the built-up areas and surrounding land cover.

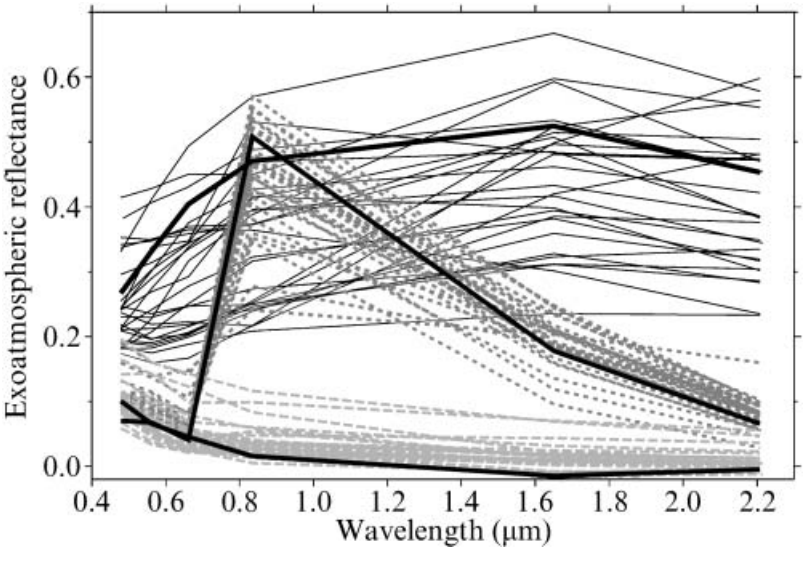

Figure 6. Spectral endmember reflectance vectors. Exoatmospheric reflectances correspond to pixels at the apexes of the mixing spaces shown in figure 3. Heavy solid curves are the global endmembers from the global mixing space shown in figure 4. Even without radiometric rectification or atmospheric correction, the Dark (long dash) and Vegetation (short dash) endmembers are remarkably consistent in shape while variable in amplitude. The High Albedo (solid) endmembers are quite variable in amplitude but generally show a convex upward shape with peak reflectance at SWIR wavelengths.

the Dark endmember was chosen to correspond to clear water or deep shadow areas. The short wavelength curvature of these Dark reflectances shows the atmospheric path radiance component that is present in every pixel. The fraction of Dark endmember is inversely related to the overall albedo of a mixed pixel because it represents atmospheric scattering in the absence of surface reflectance. The fraction of High Albedo endmember does not necessarily provide an accurate estimate of the overall albedo because of the non-linearity and dispersion of most mixing spaces near the high albedo apex. The high intra- and interurban variability of the High Albedo endmember suggests that a single endmember could not accurately represent the wide variety (but low areal abundance) of high albedo reflectances observed. For the same reason, the similarity of the Dark endmember suggests that it provides a more consistent inverse metric of overall urban albedo.

Consistency in the topology of spectral mixing spaces is also reflected in the consistency in variance partition seen in eigenvalue distributions (figure 4). Analysis of AVIRIS hyperspectral imagery indicates that urban spectral dimensionality can be scale dependent as larger areas can contain a wider variety of spectral endmembers (Small 2001b). Because surrounding areas may be more spectrally diverse than the built-up area, mixture analyses were also conducted for 5 km × 5 km and 1 km × 1 km areas around the city centres. The eigenvalue distributions for these smaller subsets also indicate that the mixing space is essentially two-dimensional. Note that the global endmembers do not bound all of the scene-specific local endmembers but do have a consistent shape. The consequences of this are discussed below.

Inversion of the three-endmember linear mixture model with the global endmembers results in reasonably low misfits between observed and modelled reflectance. The unity-constrained, least squares inversion, described in Small (2001a), was applied to all 28 images using both scene specific and global endmembers. Mixed pixel reflectance is forward modelled by summing the fraction estimate weighted endmembers for comparison to the observed reflectance vector on which the fraction estimate is based. RMS misfit between the modelled and observed reflectances provides a quantitative measure of how well the estimated fractions and endmembers can reproduce the observed reflectance. The distributions of RMS misfit are normalized by the mean reflectance amplitude for each pixel of each image (figure 7). The misfits are normalized to better reflect the relative magnitude of the misfit to the observed reflectance. Un-normalized misfit distributions convey an overly optimistic impression of small misfit in images with large areas of low amplitude reflectance. Scaling the misfit by the mean amplitude for each pixel provides a better indication of the magnitude of the misfit relative to the amplitude of the corresponding mixed pixel. Nonetheless, all but two of the 28 images have median misfits less than 10% of the mean reflectance amplitude. The two images with larger misfits are Taipei and San Salvador. The misfits in the Taipei image result from a large cloud in the middle of the image. As expected, the complex reflectance of the cloud is not well fit by the simple three-endmember linear model. The larger misfits in the Salvador image result from the pervasive presence of an unmodelled soil endmember. Large areas of fallow agricultural land surrounding Guangzhou are also not well fit and result in a bimodal misfit distribution with a small mode near 0.25.

The fraction estimates derived from the global endmembers show a strong linear correspondence to the estimates derived from the local, scene-specific, endmembers.

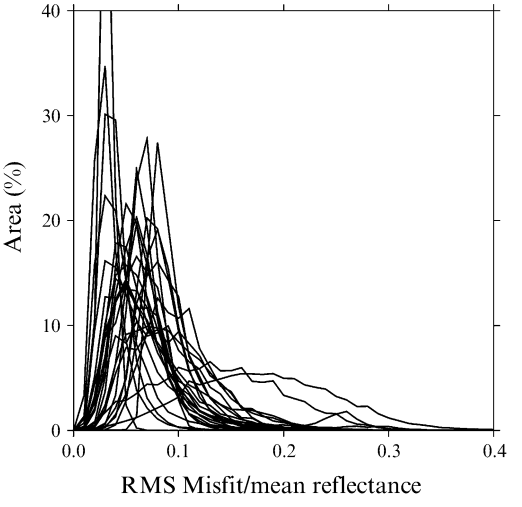

Figure 7. Normalized misfit distributions for the three-endmember linear mixture model. All but two of the 28 urban areas have a median misfit of less than 10% of the mean amplitude of the corresponding pixel. The two images with higher misfit (San Salvador and Taipei) result from large areas of unmodelled soil and cloud (respectively) endmembers.

Figure 8 shows scatter plots of fraction estimates for four contrasting cases of strong and somewhat weaker correspondence between global and local endmember fractions. The width or dispersion of the scatter plot indicates the degree of correspondence between the global and local endmember fraction estimates. The slope of the linear scatter plot shows the amplitude correspondence. Perfect agreement would yield a narrow diagonal scatter plot along the 1:1 line. Slopes less than 1:1 indicate a local endmember that does not span the full range of the corresponding global endmember. In this example, Cairo and Damascus show strong linear relationships but differing amplitude correspondence. Cairo's global fraction of High Albedo endmember saturates at 77% of the local high albedo fraction while Lagos' local high albedo fraction saturates at 63% of the global high albedo fraction and bottoms at 24%. In part, this is a result of Cairo's clear atmosphere and large amplitude High Albedo endmember (relative to the global High Albedo endmember) and Lagos' turbid atmosphere that reduces the amplitude (by absorption) of the High Albedo endmember and increases (by scattering) the amplitude of the Dark endmember. The high minimum values of Lagos' global Dark endmember also indicates the high level of atmospheric path radiance relative to the other cities (except Tianjin). Similarly, both Lagos and Tianjin have severely attenuated local Vegetation endmembers relative to the other cities. Tianjin has a strong linear correspondence in the dark and vegetation fractions but a weaker correspondence in the high albedo fraction. Damascus has considerably more scatter for all fractions, suggesting a weaker linear correspondence between global and local endmembers than the other cities. Damascus' higher local misfit suggests that the local endmembers do not fit the observations as well as the global endmembers. Lagos has a multimodal misfit distribution with a subset of pixels that are well fit by the local endmembers but poorly fit by the global endmembers. The strong linear relationship between global and local endmember fraction estimates suggests that this type of misfit analysis could yield scaling factors for mapping

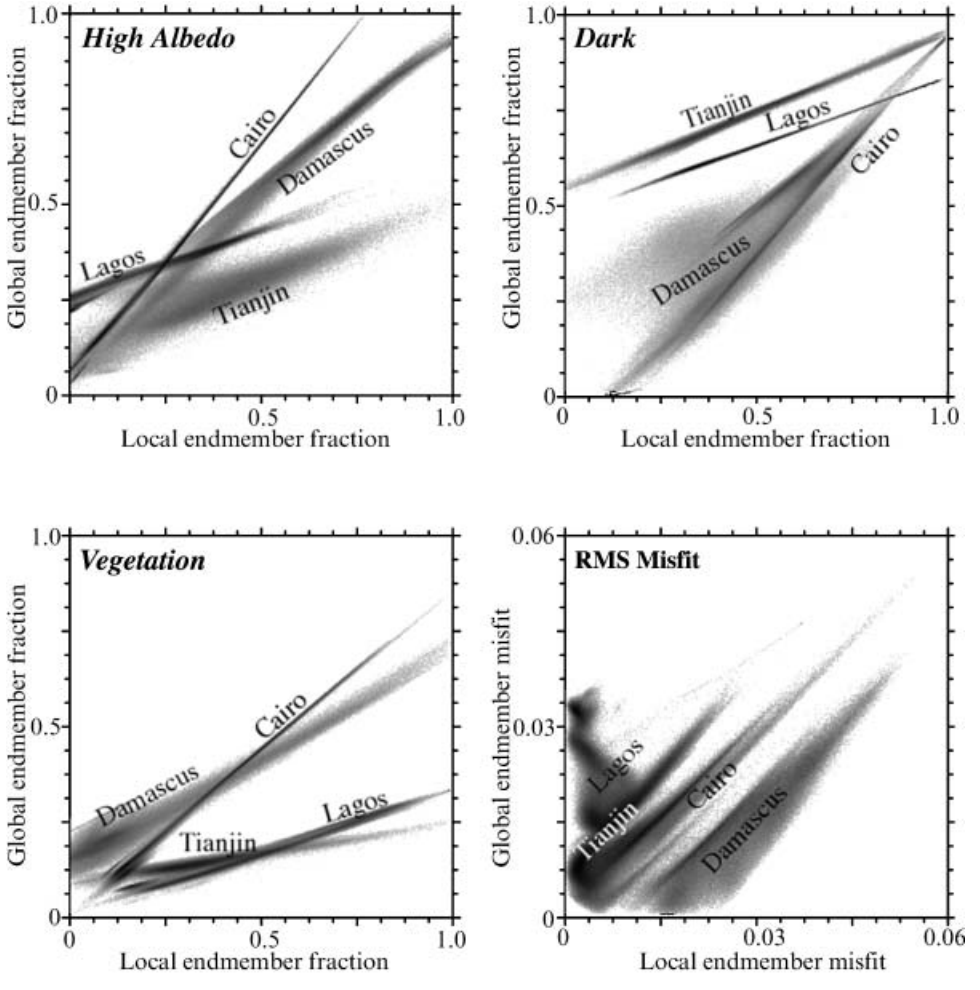

Figure 8. Scatter plots of endmember fraction estimates derived from global endmembers and local, scene-specific endmembers. The dispersion and linearity of each scatter plot indicates the extent to which the global and local endmembers are linearly related. The slope of each scatter plot shows the extent to which the local endmembers overestimate (e.g. Cairo – High Albedo) or underestimate (e.g. Lagos – High Albedo) the global fractions. The positive intercepts of the Dark scatter plots (Tianjin and Lagos) result from atmospheric path radiance.

calibrated local endmember fractions to globally consistent fraction estimates. Specifically, the zero intercept of the Dark endmember could provide an indication of the local path radiance relative to a global endmember from a relatively clear atmosphere. This type of analysis also provides a way to flag urban images with severe atmospheric turbidity or poorly constrained endmembers.

Comparison of the average endmember fractions of the 28 urban areas suggests considerable variability in urban reflectance. Figure 9 shows average endmember fractions plotted on ternary diagrams for both the $30\,\text{km} \times 30\,\text{km}$ and $5\,\text{km} \times 5\,\text{km}$ images. Much of the variability in the $30\,\text{km} \times 30\,\text{km}$ images results from the wide range of land cover types surrounding the urban areas. The $5\,\text{km} \times 5\,\text{km}$ images more accurately reflect the spectral characteristics of the built-up areas of each city.

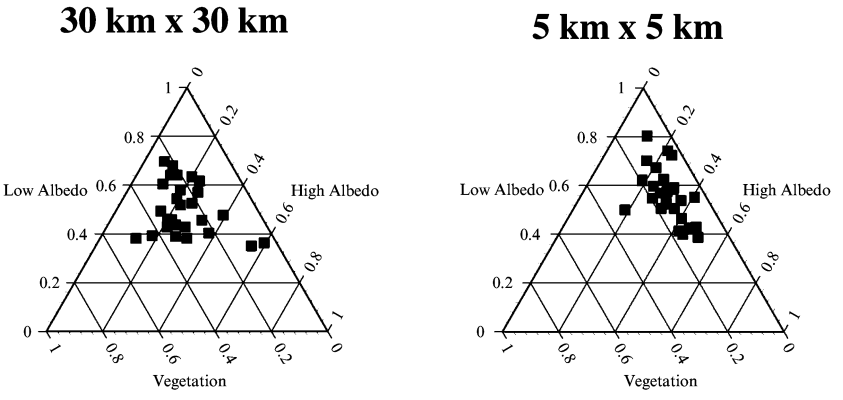

Figure 9. Ternary diagrams showing average endmember fractions for the 28 urban areas and city centres. Average fractions of the 30 km × 30 km images are heavily influenced by land cover surrounding the urban area. Average fractions for the 5 km × 5 km city centres are more representative of the built-up area and are displaced toward the Dark endmember along the grey axis with less than 20% vegetation fraction. The wide range of average fractions indicates considerable intraurban spectral variability.

The average endmember fractions of the 5 km × 5 km images are distributed along the grey axis between the High Albedo and Dark endmembers. Vegetation fractions in city centres are less than 20% on average. Some of this variability is related to differences in atmospheric conditions but the range of fractions is larger than the atmospherically induced variability implied by figure 8. Based on these plots, there is no evidence to suggest the existence of a single characteristic urban reflectance signature for the built environment. This is not surprising given the diversity of structures and building materials used in urban areas.

5. Discussion

The preceding analysis suggests that three-endmember linear mixture models are well posed for the urban areas investigated in this study. Some areas could be represented more accurately with four-endmember models but, in general, the RMS misfits to the three-endmember models are small (>0.1 of mean pixel reflectance in figure 7). Small misfit is a necessary but not sufficient verification of the linear mixture model. Large misfits would indicate that the model did not provide an accurate description of the mixed reflectances but small misfit does not guarantee that the estimates are accurate areal measures of specific land cover types. This requires field validation with actual endmember fraction measurements. Vegetation fraction estimates derived from Landsat 5 imagery agree with high spatial resolution (2 m) measurements of areal vegetation cover to within 10% in New York (Small 2001a) so there is some basis for expecting correspondence in other cities. Additional field validation will be necessary to determine if this level of accuracy can be obtained for other endmembers in other urban settings. Nonetheless, the low misfits do suggest that the three-endmember model can account for most of the observed variance. As such, it provides a simple, accurate and robust way to characterize urban reflectance.

Endmember fraction estimates are related to Tasselled Cap Brightness and Greenness (Kauth and Thomas 1976). Figure 11 shows the strong similarity between

the global mixing space and a scatter plot of the Tasselled Cap Brightness and Greenness. The first principal component of the global composite has a correlation of 0.99 with the Brightness image and the second principal component has a correlation of 0.94 with the Greenness image. In spite of the strong correlation to endmember fractions, Tasselled Cap components do not provide physical quantities that can be directly calibrated. Furthermore, greenness and brightness are not truly independent quantities. As pointed out by Jackson (1983), both greenness and brightness depend on soil reflectance so the greenness does not necessarily provide an independent measure of the amount of vegetation present. In many of the urban areas the Tasselled Cap rotation produces nonsensical results in which a single greenness value often corresponds to a variety of land cover types–including some on the grey axis (soil line) that presumably contain no vegetation. This is particularly evident in arid settings like Cairo and Damascus where unvegetated, high albedo areas end up with moderate greenness values. In contrast, the spectral endmembers are constrained to sum to unity, are more nearly orthogonal (figure 10) and are directly related to the physical components contributing to the mixed radiance measurements. Endmembers chosen to bound the global mixing space will still produce estimates that are linearly related to the scene-specific endmembers so they can easily be calibrated with validation measurements (Small 2001a).

One of the primary advantages of the linear mixture model is the straightforward physical interpretation. Representing the urban mosaic as combinations of High Albedo, Dark and Vegetation reflectance is a gross simplification but it accurately represents the most important physical properties of the surface reflectance of a wide variety of developed and undeveloped land cover types. The consistency of the three-endmember urban mixing space has been verified both at higher spectral resolution with AVIRIS hyperspectral imagery and at higher spatial resolution with Ikonos imagery (Small 2001c). It is, however, important to remember that the Landsat mixing space is a low dimensional projection of a higher dimensional mixing space. Because the Landsat sensor lacks the spatial and spectral resolution necessary to discriminate the wide variety of reflectances present in the urban mosaic, each endmember may represent a variety of different materials. For instance, several distinct high albedo surfaces (e.g. concrete, sand, gravel) can have very similar reflectance vectors when imaged by Landsat and therefore would all reside near the High Albedo endmember. The Vegetation endmember is generally the most well constrained and corresponds to grass or dense agriculture. Forest and open canopy vegetation contain an internal shade component and are represented along the mixing line between the Vegetation and Dark endmembers. The Dark endmember usually corresponds to clear water or deep shadow. Water containing suspended sediment and biological productivity is more reflective so it occurs along the mixing line between the High Albedo and Dark endmembers. The High Albedo endmember is the most compositionally variable and the least constrained by the mixing space topology. In undeveloped areas, the High Albedo endmember usually corresponds to rock or soil with high SWIR reflectance but the divergence of the mixing space often results in a wide variety of spectra near the high albedo apex of the mixing space. The spectra in figure 6 show the range of High Albedo endmembers selected for each of the 28 images. This variability detracts from the accuracy of estimates for pixels with large High Albedo fractions but this error diminishes in proportion to the High Albedo fraction so its overall impact on urban reflectance estimates is relatively small.

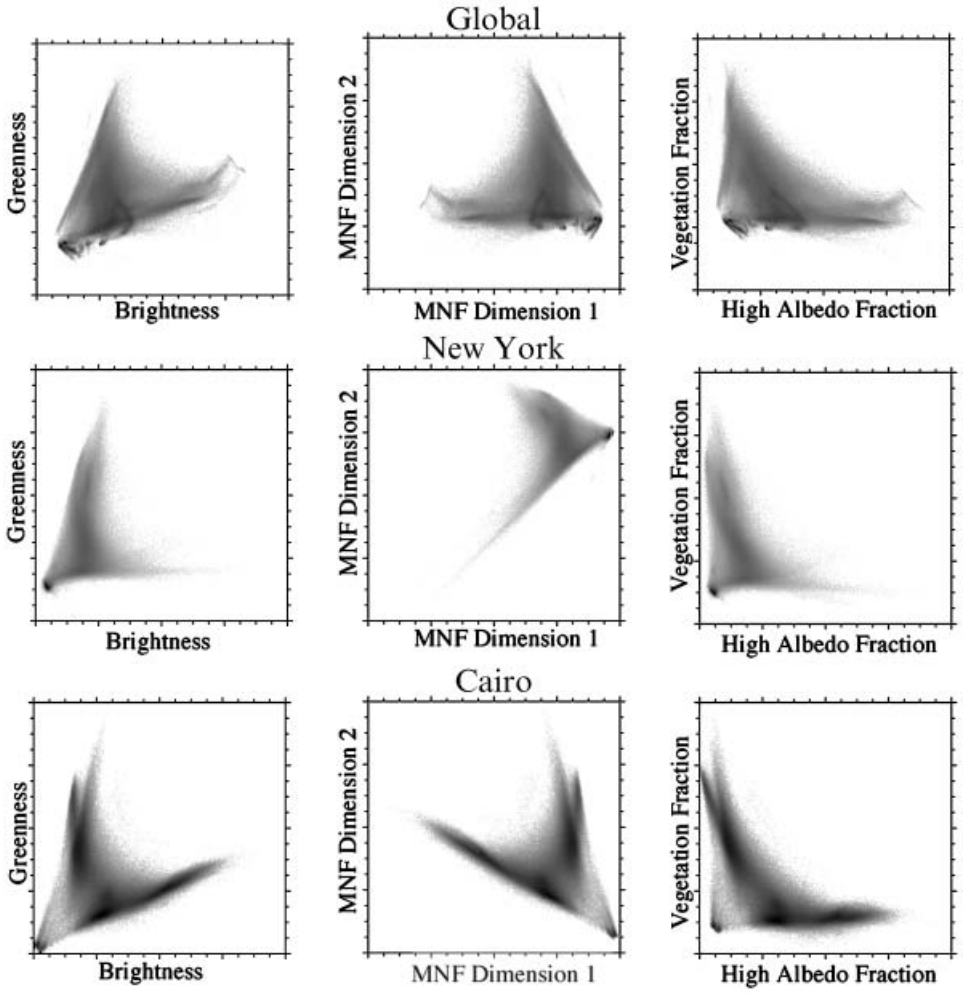

Figure 10. Comparison of Tasselled Cap Brightness and Greenness with low order principal components and endmember fractions. Aside from the reversed polarity of the first principal component, the first two components of the global composite are very similar to the Tasselled Cap Brightness and Greenness. In the New York image, the grey axis (soil line) is almost perpendicular to the Greenness component but it is not parallel to the brightness dimension in the global image. In the case of the Cairo image, the grey axis has almost equal components of Brightness and Greenness. In all three cases the High Albedo and Vegetation endmember fraction distributions are orthogonal.

The principal finding of this analysis is that built-up urban areas occupy different but distinct regions of a common spectral mixing space. In spite of the diversity of urban settlements and land cover types, the three-endmember linear model can represent the mixed radiance that results from them reasonably well. There is, however, significant variability in urban reflectance, both within and among cities. In each case the majority of the pixels in the built-up urban centre occupy a distinct region within both the local and global mixing spaces. Figure 11 shows some comparative examples of mixing space clustering of different urban centres. The example pairs where chosen to illustrate cities with both similar and different mixing spaces. Combining contrasting pairs of cities in the same mixing space highlights the

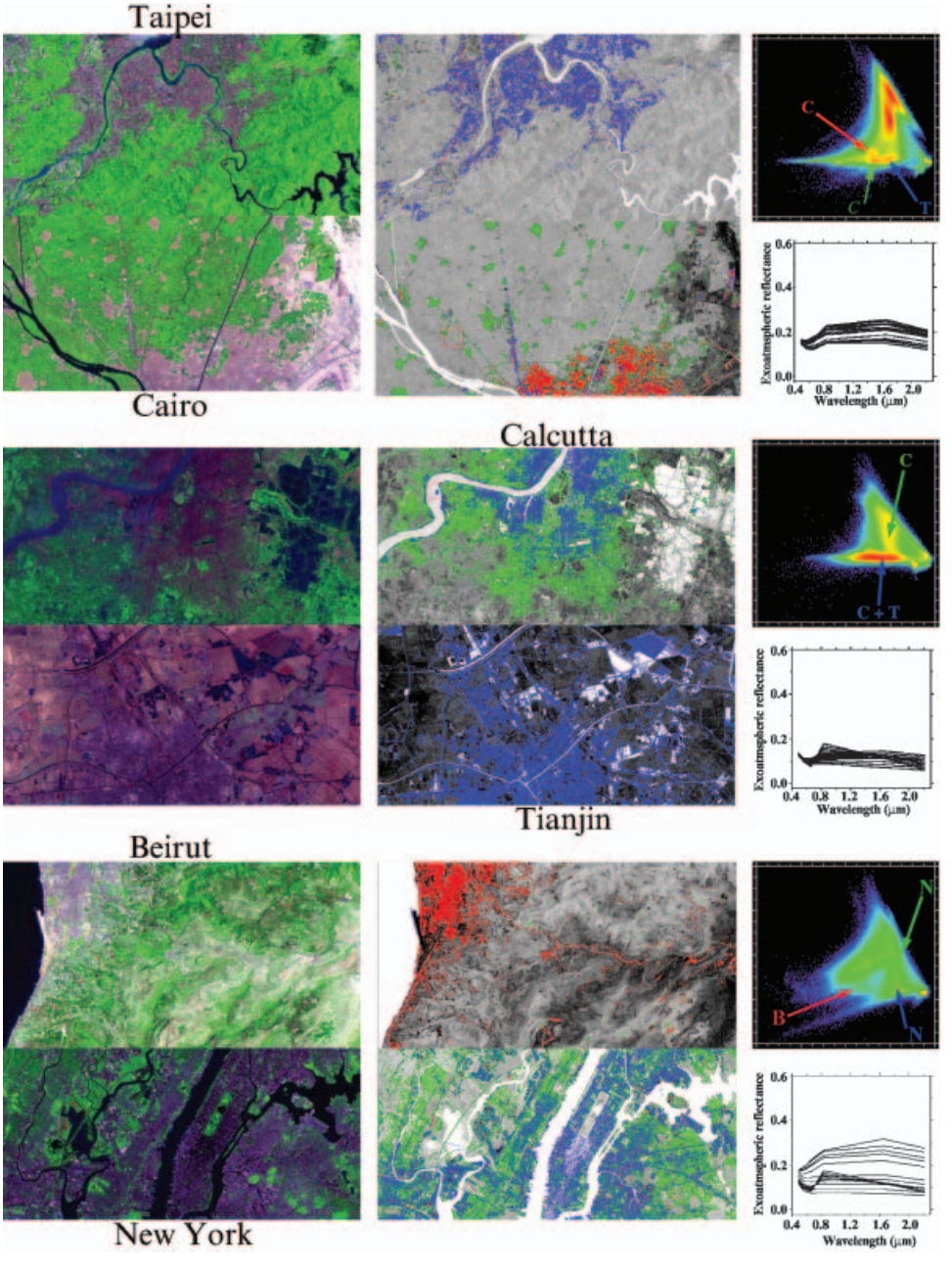

Figure 11. Mixing space separability of urban reflectance. Contrasting examples of urban reflectance are illustrated with composite scatter plots highlighting the localization of built-up urban cores in the global mixing space. Each scatter plot shows the subset of the global mixing space corresponding to 1 000 000 pixels from the pair of urban area images shown to its left. Arrows point to localized clusters of urban reflectances corresponding to the highlighted areas on the grey shade image. Reflectance vectors show spectra extracted along transects across each mixing space cluster. Most built-up areas occupy distinct parts of the mixing space but there is some overlap, as seen in Calcutta and Tianjin.

spectral similarities and differences. Each mixing space in figure 11 represents 1 000 000 pixels equally divided between the two cities in the adjacent global composite image. Cairo has two distinct clusters corresponding to the smaller settlements in the adjacent Nile delta and to the city itself. Both of these are distinct from the lower albedo Taipei cluster but some of the large thoroughfares in Cairo are spectrally similar to Taipei. In contrast, Calcutta and Tianjin share part of a single elongate cluster on the grey axis while other parts of Calcutta correspond to a mixing line between the Vegetation endmember and the grey axis. New York is also characterized by two distinct mixing lines while Beirut occupies a single distinct cluster with a greater high albedo component. The reflectance vectors show the spectral progression along these mixing lines and within the clusters. The urban pixels highlighted in each example correspond to the specific clusters in the mixing space indicated by the arrows. The spectral extent of the cluster highlighted in the mixing space determines the geographic extent of pixels highlighted on the image. In this example, these extents are selected arbitrarily to illustrate the correspondence of specific regions of the mixing space to the built-up areas visible on the adjacent false colour image.

The implication of spectral clustering is spectral consistency. This consistency can facilitate discrimination of built-up urban areas. In spite of the spectral heterogeneity at pixel scales, urban areas are distinguishable from undeveloped land cover within the mixing space. In fact, it is often the heterogeneity of urban land cover that distinguishes it from other land covers that are more spectrally pure and occupy distinct domains within the mixing space closer to the endmembers. Figure 11 indicates that compact regions in the mixing space correspond to quasi-continuous urban centres in geographic space. In contrast, continuous geographic areas generally contain a wide range of spectral mixtures, including many spectrally pure pixels residing at the periphery of the mixing space. This explains the low accuracies that often result when traditional supervised classification is applied to urban areas. The choice of a single urban class on the basis of geographically continuous training areas can combine a wide variety of mixed and pure reflectances which generate a diffuse likelihood function that overlaps many other classes thereby generating errors of both omission and commission.

Characterizing urban reflectance as spectral mixtures can provide a basis for mapping urban areas with moderate resolution multispectral imagery. Urban areas almost always contain a variety of pixels spanning a wide range of mixing fractions but this study indicates that a majority of them often correspond to a distinct cluster of spectrally heterogeneous pixels within the mixing space. This would suggest that built-up areas could be isolated in mixing space more effectively than in geographic space thereby producing a conservative classification of the mixed pixels while avoiding errors of commission resulting from overly inclusive likelihood functions. If a continuous urban area classification is required, the incomplete (granular) geographic classification could be morphologically closed by filling holes (reclassifying interstitial endmember pixels with the majority neighbour class). This could be done within a prescribed size range to preserve large intraurban features like parks. This would produce a spectrally based classification that could accommodate the spectral heterogeneity that is characteristic of urban areas worldwide. In fact, the consistency of the mixing spaces and the granularity of the urban areas in this study suggests that spectral heterogeneity may be the most characteristic feature of urban reflectance.

This analysis also highlights the diffuse nature of urban areas and the complexity of the urban-rural transition. The spectral transition spans the heterogeneous city centres along the grey axis within the mixing space as well as the more homogeneous undeveloped surrounding areas at the periphery of the mixing space. In most cases this transition occurs across a finite distance rather than abruptly at a sharp urban-rural boundary. In temperate developed countries this transition often corresponds to a vegetation gradient from sparsely vegetated city centres, through increasingly vegetated suburbs, to more densely vegetated forests and agricultural areas at their periphery. Representing reflectance as endmember fractions makes it possible to classify urban areas and their transitional surroundings on the basis of a continuous field variable, such as vegetation fraction or albedo. Continuous field variables can more accurately represent the true 'fuzzy' nature of complex entities like cities. SMA provides a physically based analogue to fuzzy classification thereby avoiding the unrealistic thresholds required by traditional 'hard' classification schemes in which each pixel receives a single binary class assignment. In this sense, continuous fields better represent the true nature of urban areas characterized by scale-dependent transitions between different combinations of land use. By accommodating heterogeneity, a continuum definition of urban areas may provide a more flexible and accurate depiction of spectral properties as well as the other physical and even socio-economic parameters that define cities.

References

ADAMS, J.B., SMITH, M.O. and JOHNSON, P.E., 1986, Spectral mixture modeling: a new analysis of rock and soil types at the Viking Lander 1 Site. *Journal of Geophysical Research*, **91**, pp. 8089–8122.

ADAMS, J.B., SMITH, M.O. and GILLESPIE, A.R., 1993, Imaging spectroscopy—Interpretation based on spectral mixture analysis. In *Remote geochemical analysis—Elemental and mineralogical composition*, C.M. Pieters and P. Englert (Eds) (New York: Cambridge University Press), pp. 145–166.

ADAMS, J.B., SABOL, D.E., KAPOS, V., FILHO ROBERTS, R.A.D.A., SMITH, M.O. and GILLESPIE, A.R., 1995, Classification of multispectral images based on fractions of endmembers: application to land cover change in the Brazilian Amazon. *Remote Sensing of Environment*, **52**, pp. 137–154.

BERRY, B.L., 1990, Urbanization. In *The Earth as Transformed by Human Action*, B.L. Turner II, W.C. Clark, R.W. Kates, J.F. Richards, J.T. Matthews and W.B. Meyer (Eds) (Cambridge: Cambridge University Press), pp. 103–119.

BATTY, M. and LONGLEY, P., 1994, *Fractal Cities* (San Diego, CA: Academic Press).

BOARDMAN, J.W., 1989, Inversion of imaging spectrometry data using singular value decomposition. *Proceedings of the 12th Canadian Symposium on Remote Sensing*, Vancouver British Columbia, pp. 2069–2072.

BOARDMAN, J., 1990, Inversion of high spectral resolution data. *SPIE—Imaging Spectroscopy of the Terrestrial Environment*, **1298**, pp. 222–233.

CHAMEIDES, W.L., KASIBHATLA, P.S., YIENGER, J. and LEVY, H.H., 1994, Growth of continental scale metro-agro-plexes, regional ozone pollution and world food production. *Science*, **264**, pp. 74–75.

ELMORE, A.J., MUSTARD, J.F., MANNING, S.J. and LOBELL, D.B., 2000, Quantifying vegetation change in semiarid environments: precision and accuracy of spectral mixture analysis and the normalized difference vegetation index. *Remote Sensing of Environment*, **73**, pp. 87–102.

FORSTER, B., 1983, Some urban measurements from Landsat data. *Photogrammetric Engineering and Remote Sensing*, **49**, pp. 1693–1707.

GILLESPIE, A.R., SMITH, M.O., ADAMS, J.B., WILLIS, S.C., FISCHER, A.F. and SABOL, D.E., 1990, Interpretation of residual images—Sprectral mixture analysis of AVIRIS images. In *Proceedings of the 2nd Airborne Visible/Infrared Imaging Spectrometer (AVIRIS) Workshop, Owens Valley, California* (Pasadena, CA: NASA Jet Propulsion Laboratory), pp. 243–270.

GREEN, A.A., BERMAN, M., SWITZER, P. and CRAIG, M.D., 1988, A transformation for ordering mutispectral data in terms of image quality with implications for noise removal. *IEEE Transactions on Geoscience and Remote Sensing*, **26**, pp. 65–74.

GREEN, R.O. and BOARDMAN, J., 2000, Exploration of the relationship between information content and signal/noise ratio and spatial resolution in AVIRIS spectral data. *Proceedings of the Ninth JPL Airborne Earth Science Workshop, NASA Jet Propulsion Laboratory Pasadena, CA*, R.O. Green (Ed.), pp. 195–206.

JACKSON, R.D., 1983, Spectral indices in n-space. *Remote Sensing of Environment*, **13**, pp. 409–421.

JENSEN, J.R. and COWEN, D.C., 1999, Remote sensing of urban suburban infrastructure and socio-economic attributes. *Photogrammetric Engineering and Remote Sensing*, **65**, pp. 611–622.

JOHNSON, P.E., SMITH, M.O. and ADAMS, J.B., 1985, Quantitative analysis of planetary reflectance spectra with principal components analysis. *Journal of Geophyical Research*, **90**, pp. C805–C810.

JOHNSON, P.E., SMITH, M.O., TAYLOR-GEORGE, S. and ADAMS, J.B., 1983, A semiempirical method for analysis of the reflectance spectra of binary mineral mixtures. *Journal of Geophysical Research*, **88**, pp. 3557–3561.

KAUTH, R.J. and THOMAS, G.S., 1976, The Tasseled Cap—a graphic description of the spectral-temporal development of agricultural crops as seen by Landsat. *Proceedings of the Symposium on Machine Processing of Remotely Sensed Data, Purdue University, West Lafayette, Indiana*, pp. 4B41–4B51.

KRESSLER, F. and STEINNOCHER, K., 1996, Change detection in urban areas using satellite images and spectral mixture analysis. *International Archives of Photogrammetry and Remote Sensing. Vol. XXXI, Part B7, Vienna, Austria, 1996*, pp. 379–383.

KRESSLER, F. and STEINNOCHER, K., 2001, Monitoring urban development using satellite images. In *Remote Sensing in Urban Areas/Fernerkennung in Urbanen Räumen—Regensburger Geographische Schriften*, J. Carslen (Ed.), **35**, pp. 140–147.

MAKSE, H.A., ANDRADE, J.S., BATTY, M., HAVLIN, S. and STANLEY, H.E., 1998, Modeling urban growth patterns with correlated percolation. *Physical Review E*, **58**, pp. 7054–7062.

NASH, E.B. and CONEL, J.E., 1974, Sprectral reflectance systematics for mixtures of powdered hypersthene, labradorite and ilmenite. *Journal of Geophysical Research*, **79**, pp. 1615–1621.

NORDBECK, S., 1971, Urban allometric growth. *Geografiska Annaler*, **53B**, pp. 54–67.

PECH, R.P., DAVIES, A.W., LAMACRAFT, R.R. and GRAETZ, R.D., 1986, Calibration of Landsat data for sparsely vegetated semi-arid rangelands. *International Journal of Remote Sensing*, **7**, pp. 1729–1750.

RASHED, T., WEEKS, J.R., STOW, D. and FUGATE, D., 2002, Measuring temporal compositions of urban morphology through Spectral Mixture Analysis: toward a soft approach to change analysis in crowded cities. *Proceedings of the Third International Symposium on Remote Sensing of Urban Areas, Istanbul, Turkey, 11–13 June, 2002*, pp. 512–527.

RESEARCH SYSTEMS INC., 2000, *ENVI 3.4. User's Guide* (Boulder, Colorado), p. 930.

ROBERTS, D.A., BATISTA, G., PEREIRA, J., WALLER, E. and NELSON, B., 1998, Change identification using multitemporal spectral mixture analysis: applications in eastern Amazonia. In *Remote Sensing Change Detection: Environmental Monitoring*

Applications and Methods, C. Elvidge and R. Lunetta (Eds) (Ann Arbor: Ann Arbor Press), pp. 137–161.

SINGER, R.B., 1981, Near-infrared spectral reflectance of mineral mixtures—systematic combinations of pyroxenes, olivie and iron oxides. *Journal of Geophysical Research*, **86**, pp. 7967–7982.

SINGER, R.B. and MCCORD, T.B., 1979, Large scale mixing of bright and dark surface materials and implications for analysis of spectral reflectance. *Journal of Geophysical Research*, pp. 1835–1848.

SMALL, C., 2001a, Estimation of urban vegetation abundance by spectral mixture analysis. *International Journal of Remote Sensing*, **22**, pp. 1305–1334.

SMALL, C., 2001b, Spectral dimensionality of urban radiance. *Proceedings of 10th JPL Airborne Earth Science Workshop, NASA Jet Propulsion Laboratory, Pasadena, CA*, pp. 375–385.

SMALL, C., 2001c, Multiresolution analysis of urban reflectance. *Proceedings of the IEEE Joint Workshop on Remote Sensing and Data Fusion over Urban Areas, 8–9 November 2001, Rome, Italy*, paper 23.

SMALL, C., 2002, Multitemporal analysis of urban reflectance. *Remote Sensing of Environment*, **81**, pp. 427–442.

SMALL, C., 2003, High resolution spectral mixture analysis of urban reflectance. *Remote Sensing of Environment*, **88**, pp. 170–186.

SMITH, M.O., JOHNSON, P.E. and ADAMS, J.B., 1985, Quantitative determination of mineral types and abundances from reflectance spectra using principal component analysis. *Journal of Geophysical Research*, **90**, pp. C792–C804.

SMITH, M.O., USTIN, S.L., ADAMS, J.B. and GILLESPIE, A.R., 1990, Vegetation in deserts: I. A regional measure of abundance from multispectral images. *Remote Sensing of Environment*, **31**, pp. 1–26.

STEFANOV, W.L., RAMSEY, M.S. and CHRISTENSEN, P.R., 2001, Monitoring urban land cover change: an expert system approach to land cover classification of semiarid to arid urban centers. *Remote Sensing of Environment*, **77**, pp. 173–185.

UNITED NATIONS, 2002, *World Urbanization Prospects—The 2001 Revision* (New York: United Nations Population Division).

ZANETTE, D.H. and MANRUBIA, S.C., 1997, Role of intermittency in urban development: a model of large scale city formation. *Physical Review Letters*, **79**, pp. 523–526.